Water Mass Transformation and Overturning Circulation in the Arabian Gulf

MARYAM R. AL-SHEHHI,[a] HAJOON SONG,[b] JEFFERY SCOTT,[c] AND JOHN MARSHALL[c]

[a] *Civil and Environmental Engineering, Khalifa University, Abu Dhabi, United Arab Emirates*
[b] *Department of Atmospheric Sciences, Yonsei University, Seoul, South Korea*
[c] *Department of Earth, Atmospheric, and Planetary Sciences, Massachusetts Institute of Technology, Cambridge, Massachusetts*

ABSTRACT: We diagnose the ocean's residual overturning circulation of the Arabian Gulf in a high-resolution model and interpret it in terms of water-mass transformation processes mediated by air–sea buoyancy fluxes and interior mixing. We attempt to rationalize the complex three-dimensional flow in terms of the superposition of a zonal (roughly along axis) and meridional (transverse) overturning pattern. Rates of overturning and the seasonal cycle of air–sea fluxes sustaining them are quantified and ranked in order of importance. Air–sea fluxes dominate the budget so that, at zero order, the magnitude and sense of the overturning circulation can be inferred from air–sea fluxes, with interior mixing playing a lesser role. We find that wintertime latent heat fluxes dominate the water-mass transformation rate in the interior waters of the Gulf leading to a diapycnal volume flux directed toward higher densities. In the zonal overturning cell, fluid is drawn in from the Sea of Oman through the Strait of Hormuz, transformed, and exits the Strait near the southern and bottom boundaries. Along the southern margin of the Gulf, evaporation plays an important role in the meridional overturning pattern inducing sinking there.

KEYWORDS: Buoyancy; Mixing; Ocean circulation; Streamflow; Thermocline circulation; Upwelling/downwelling

1. Introduction

In this paper, we map and quantify the transformation of water masses by air–sea interaction and interior mixing in a high-resolution simulation of the Arabian Gulf (hereafter referred to as the Gulf). The Gulf is a marginal sea of the Arabian Sea that extends from the Sea of Oman in the south to the Shatt Al-Arab in the north with a length of approximately 1000 km (Fig. 1). It is a shallow, evaporative basin with a depth that rarely exceeds 90 m connected to the very much deeper (>2000 m) Sea of Oman through the Strait of Hormuz. The restricted exchange with the open ocean through the Strait leads to the formation of a saline, dense water mass which flows out, with fresher waters from the Sea of Oman being drawn in at the surface (see, e.g., Swift and Bower 2003; Vasou et al. 2020). This system corresponds to an anti-estuarine circulation (Reynolds 1993; Swift and Bower 2003) with an exchange volume flux of $O(0.1)$ Sv (1 Sv $\equiv 10^6\,\mathrm{m}^3\,\mathrm{s}^{-1}$) (Johns et al. 2003; Yao and Johns 2010) and a bottom water flushing time scale of 3 years or so (Sadrinasab and Kämpf 2004).

The circulation in the eastern part of the Gulf is characterized by a cyclonic gyre fed by relatively freshwater from the Sea of Oman compared to that within the Gulf (Reynolds 1993; Johns et al. 2003; Pous et al. 2013). While the fluid circulates around the Gulf, it loses buoyancy due to excessive evaporation and associated latent heat loss (Madani et al. 2012). The desalination plants populated along the south coast further densify the Gulf by brine discharge (Ibrahim and Eltahir 2019). The flow of dense water out of the Gulf is mostly confined to the bottom on the southern side of the Gulf (Swift and Bower 2003).

The cyclonic circulation evolves over the course of the year. The surface currents are strongest in summer and flow from the central Gulf toward the southern shallows (Hosseinibalam et al. 2011). Then the cyclonic gyre breaks down into smaller mesoscale eddies as is evident in both satellite observations and numerical models (Sadrinasab and Kämpf 2004; Thoppil and Hogan 2010a; Pous et al. 2015). The current is weakest in winter due to reduced stratification and reduced lateral density gradients between the Gulf and the Sea of Oman (Thoppil and Hogan 2010a). Tidal forcing adds a barotropic signal which dominates the background current at any instant but is less apparent when averaged over several tidal cycles (Johns et al. 2003).

In the Gulf, water masses undergo transformation from one density class to another through the action of buoyancy fluxes at the sea surface and diapycnal mixing in the interior ocean. The resulting volume fluxes between density classes play a fundamental role in the vertical overturning circulation of the ocean. A theoretical water-mass transformation framework was provided by Walin (1982) which has served useful in understanding the drivers of global and regional ocean circulation (Tziperman 1986; Speer and Tziperman 1992; Garrett et al. 1995; Marshall et al. 1999; Nishikawa et al. 2013; Badin et al. 2013; Abernathey et al. 2016; Cerovečki and Mazloff 2016). The framework is particularly useful when isopycnals outcrop and multiple layers of fluid provide direct pathways between the surface and the interior ocean. This is precisely the situation at play in the Gulf where we might anticipate active water-mass transformation and associated volume fluxes induced by evaporative processes within the Gulf itself.

Observational data are limited in the Gulf and so understanding of its circulation is enhanced through numerical simulation (Azhar et al. 2016). Early efforts focused on the general circulation in the Gulf (Chao et al. 1992), followed by more recent studies exploring seasonal variability (Kämpf and Sadrinasab 2006), the role of tides (Azam et al. 2006), mesoscale processes (Thoppil and Hogan 2010a), and the heat and salinity budgets (Johns et al. 2003; Xue and Eltahir 2015).

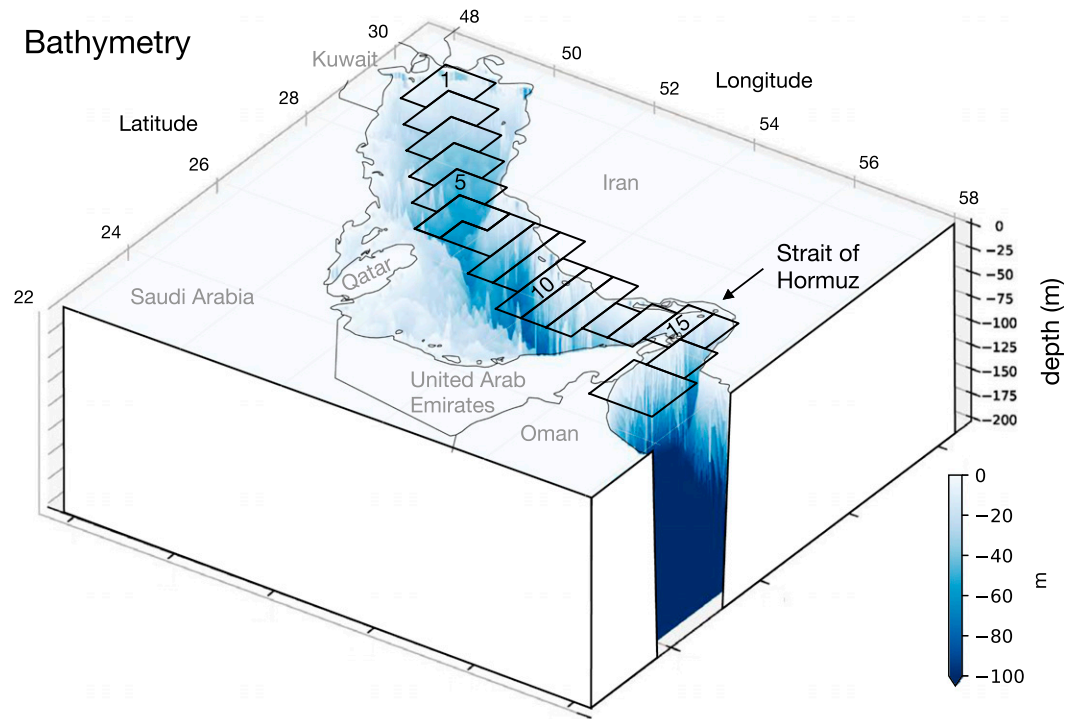*Corresponding author*: Hajoon Song, hajsong@yonsei.ac.kr

FIG. 1. The geography and bathymetry (shading in blue) of the Gulf of Arabia, together with the surrounding countries and the Strait of Hormuz marked. Eighteen black boxes, adopted from Fig. 2 in Swift and Bower (2003), are the regions over which spatial averages of in situ observations and model results are compared.

Here we attempt to visualize the complex three-dimensional circulation patterns of the Gulf using zonal and meridional overturning circulation patterns and quantify the relative roles of air–sea heat fluxes and freshwater fluxes associated with them using the Walin water-mass transformation framework. We use the MIT ocean circulation model (MITgcm), a widely used hydrodynamical model that solves the incompressible Navier–Stokes equations (Marshall et al. 1997a,b). It has been used to simulate ocean circulation over a broad range of scales, from studies with a domain on the order of 100 m to global ocean simulations, but is applied here for the first time to address the special conditions of the Gulf.

Our paper is set out as follows. In section 2 we describe the design and setup of our model, and then present the resulting water masses and circulation patterns and compare it with observations in section 3. In section 4 we analyze the water-mass transformation processes and overturning circulation patterns associated with our solution, followed by discussion and conclusions in section 5.

2. A regional model of the circulation of the Arabian Gulf

a. Global reference model

We prepared our regional model using a high-resolution global configuration of the MITgcm, the so-called LLC4320 simulation (Rocha et al. 2016; Torres et al. 2018). The global setup employs a latitude/longitude/polar cap (LLC) configuration on an Arakawa-C grid using a nominal horizontal grid spacing of

1/48°; the grid has a quasi-uniform meridional and zonal spacing of 2 km in the Gulf region, but varies between 0.8 and 2.2 km over the globe. The vertical resolution varies from a thickness of 1 m at the surface to 480 m at depth with a linearized implicit free surface. The model is stepped forward using a seventh-order monotonicity-preserving advection scheme (Daru and Tenaud 2004) and no explicit horizontal diffusivity. Horizontal viscosity and vertical mixing are parameterized using a biharmonic "modified Leith viscosity" with a vertical viscosity of $5.4 \times 10^{-4} \, \mathrm{m^2 \, s^{-1}}$ and the K-profile parameterization (KPP; Large et al. 1994) with a background diffusivity of $5.4 \times 10^{-7} \, \mathrm{m^{-2} \, s^{-1}}$, respectively. No-slip boundary conditions on the bottom and side are used.

The LLC4320 simulation was run for the calendar period from 13 September 2011 through 15 November 2012, with initial conditions taken from a hierarchy of increasingly high-resolution simulations begun from the ECCO2 state estimation (Menemenlis et al. 2008). It was forced at the surface by 6-h European Centre for Medium-Range Weather Forecasts (ECMWF) atmospheric operational model analysis at 0.14° resolution, (roughly 15 km) using bulk formulas following Large and Pond (1981). A synthetic atmospheric surface pressure field consisting of 16 tidal forcing constituents was used to dynamically mimic tidal forcing (Wang et al. 2018). Monthly river runoff was derived from Large and Nurser (2001) (see also Stammer et al. 2004).

b. Embedded model of the Gulf and Sea of Oman

Our study region is the Gulf and its connection to the Sea of Oman, as shown in Fig. 1. The regional model was embedded
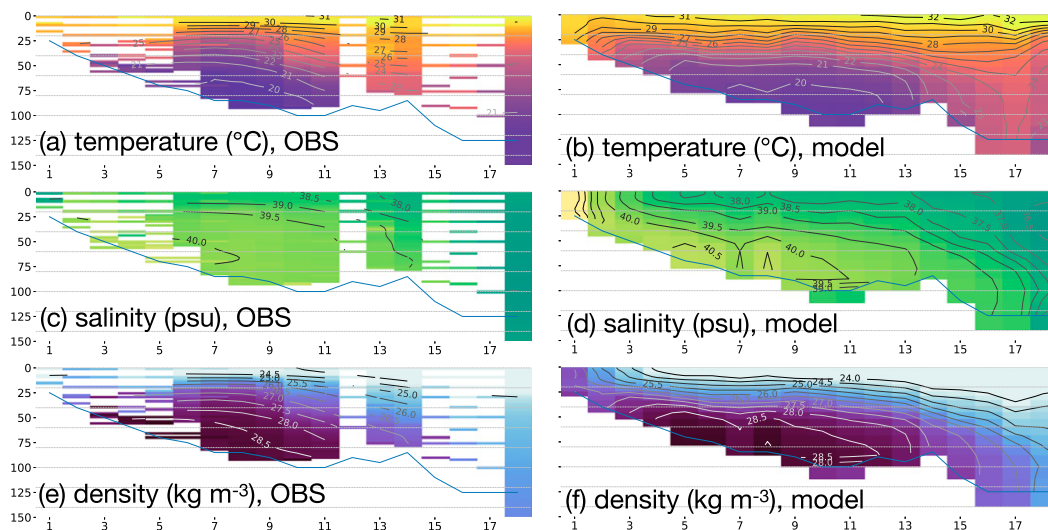
Summer

FIG. 2. Vertical sections of (a),(b) temperature, (c),(d) salinity, and (e),(f) density during summer in the boxes shown and labeled in Fig. 1. The observations on the left in (a), (c), and (e) represent the mean of in situ samples representative of the summer, July, and August. The model solution on the right in (b), (d), and (f) are spatial means over the same boxes again in summer.

within the global model described above. Starting from the global model bathymetry, modifications were made to more accurately represent coastlines. A 2-arc-min resolution bathymetry, yielding approximately 3.5 km in the Gulf, is employed based on Smith and Sandwell (1997). We used the same horizontal and vertical resolution as the global model, comprising 832 × 480 cells with 83 vertical levels. The surface forcing is identical to that of the global model and used ECMWF data for the full calendar year 2012. However, a custom monthly river freshwater outflow dataset (capturing the discharge of the Shatt Al-Arab, Mand, Hindijan, and Hilieh rivers) was configured for our modified bathymetry based on Alosairi and Pokavanich (2017). The model time step was 60 s. Open boundary conditions (currents, salinity, temperature, and sea surface height) were imposed at the southern and eastern boundaries, obtained from the global run. To improve upon the representation of the tides, 5-day running means of open boundary data from the global model were calculated, filtering out the tidal forcing signal contained in the global model. New tidal forcing components, extracted from the TPXO model, were then constructed based on Egbert and Erofeeva (2002), comprising the M_2, S_2, K_2, K_1, O_1, and P_1 tidal constituents, and were added to the southern and eastern open boundary conditions. Initialized from the global ocean state on 1 January 2012, the Gulf model was run on for a total of 6 years using repeating 2012 year forcing; the first 4 years were considered to be the spinup period and the last 2 years used for the analyses presented here.

3. Modeled circulation and hydrography in the Gulf

a. Temperature and salinity structure

The solution of the regional model is compared to in situ observations of temperature and salinity taken from the Master

Oceanographic Observations Dataset (MOODS) (Alessi et al. 1999). The data span the period 1940–90 and have a rather inhomogeneous distribution in both time and space. We therefore use seasonal-mean vertical profiles of temperature and salinity averaged within the black boxes shown in Fig. 1, following the study of Swift and Bower (2003). Although the observations remain rather sparse even after such temporal and spatial averaging, they clearly document significant seasonality in the stratification of the Gulf.

The observations reveal that in summer the Gulf is strongly stratified (Figs. 2a,c,e). The temperature can exceed 30°C at the surface yet is colder than 20° below 100 m. The salinity increases with depth but relatively slowly. The vertical structure of density closely follows that of temperature, showing that temperature plays the dominant role in setting stratification. In winter, in contrast, the temperature becomes vertically uniform (Fig. 3a). Colder temperatures can be found toward the western margin of the Gulf where it is below 19°C. This cold water mass eventually fills the bottom of the Gulf and is transported down toward the center of the Gulf in summer. The vertical distribution of salinity is less homogeneous than that of temperature and bottom waters are particularly salty in winter, exceeding concentrations of 40 psu (Fig. 3c). Since cold and salty waters are located at the innermost region of the Gulf, the density typically increases toward the bottom of the northern end of the Gulf (Fig. 3e).

Our numerical solution exhibits broad similarities with the observations. It has clear seasonality, with highly stratified water in summer while relatively homogeneous in winter. The water generally becomes saltier toward the inner Gulf in both summer and winter, which is consistent with the observations. There are also differences. The solution in summer is slightly
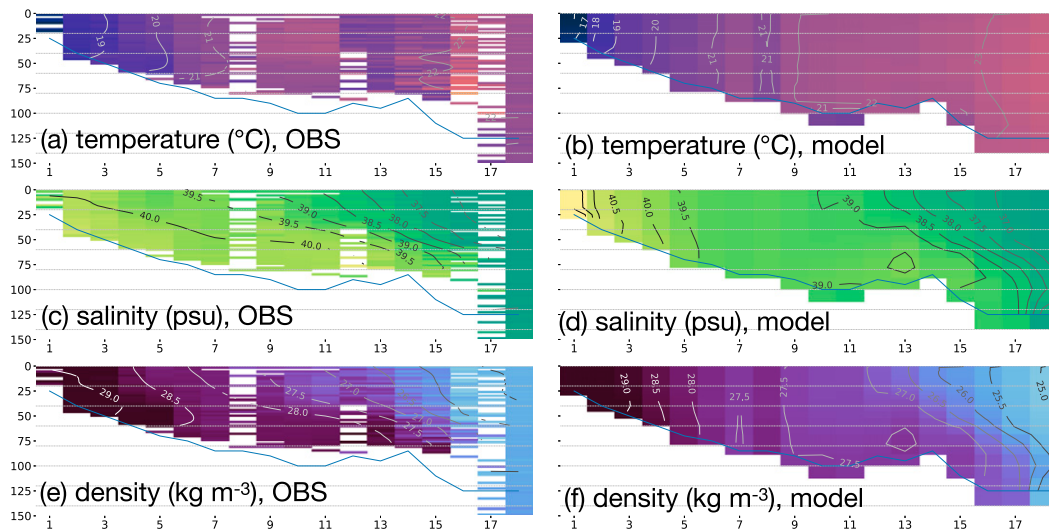
Winter

FIG. 3. As in Fig. 2, but the observations are a mean over the winter period, January, and February. (left) Observations and (right) model.

warmer and fresher than the observations at the surface near the Strait of Hormuz and most parts of the Gulf, resulting in lighter surface water (Figs. 2b,d,f). In winter, the simulated temperature and salinity are vertically uniform, indicating intense convection in the Gulf. The degree of vertical homogeneity is greater in the model than the observations, particularly in salinity. The simulated water mass at the innermost part of the Gulf is colder and saltier than the observations. This leads to an overestimate of the density in these regions (Figs. 2f and 3f). However, these differences are small compared to the magnitude of the seasonal cycle and internal variability. The water mass found near the bottom of the Gulf originates from the wintertime vertical mixing near the northern end of the Gulf when judged based on the temperature values, which is consistent with the observations. Given that our solution is driven by repeated surface forcing from a particular year while the observations span over 50 years, and the river runoff varies from year to year, there is encouraging agreement, both in the spatial pattern and seasonal cycle, between the model and in situ climatological observations.

b. Horizontal circulation patterns

Surface currents in the Gulf are characterized by a cyclonic gyre (Fig. 4). Inflow through the Strait of Hormuz into the Gulf near the northern coast, and the southeast flow from the central region of the Gulf toward the Strait, are present in both seasons (Figs. 4c,d). In summer, the surface flow is more dynamic than in winter, with a northwest current near the northern coast of the Gulf as well as a southward flow along 50°E. These horizontal circulation patterns at the surface can partially be explained by the pattern of prevailing wind stress (Figs. 4a,b). In summer, the southeastward wind stress is the strongest in the northern Gulf, and surface flow is generally to the southeast (Fig. 4c). In winter, in contrast, the maximum wind stress is

found over the center of the Gulf and is responsible for the south and southeast surface flows. In wintertime, the surface flow of both the northern Gulf and the inflow coming through the Strait of Hormuz along the northern coast significantly weaken (Hosseinibalam et al. 2011), resulting in much less distinct cyclonic flow than in the summer. It is likely that the former is caused by the wintertime wind stress which is directed opposite to the surface flow, while the latter is a consequence of a thicker surface layer with relatively uniform density at the northern end of the Gulf (Figs. 3e,f) (Thoppil and Hogan 2010b; Alosairi et al. 2011).

The barotropic streamfunction for the depth-integrated circulation in the Gulf has a dipole pattern, as can be seen in Fig. 5. Positive values are found over a broad area in the southern part of the Gulf, while negative values are found in a relatively narrow band near the northern coastal region. This indicates broad cyclonic circulation in the southern Gulf with narrow anticyclonic circulation to the north of it. Sandwiched between these two patterns is the inflow through the Strait of Hormuz which extends westward to 52°E. The vertical section of zonal velocity at the Strait (inset in Fig. 5) reveals that the inflow extends midway across, from the surface to the ocean floor, with speeds of $O(0.1)$ m s^{-1}. The existence of the outflow near the southern end of the Strait is consistent with previous observational studies (e.g., Johns et al. 2003), and the core of the outflow is bottom intensified, as seen in the observations (Schott and McCreary 2001).

4. Water-mass transformation and overturning circulation

Fluid coming in through the Strait of Hormuz is transformed by air–sea fluxes and mixing within the Gulf, so that fluid exiting from the Strait has properties which are different from
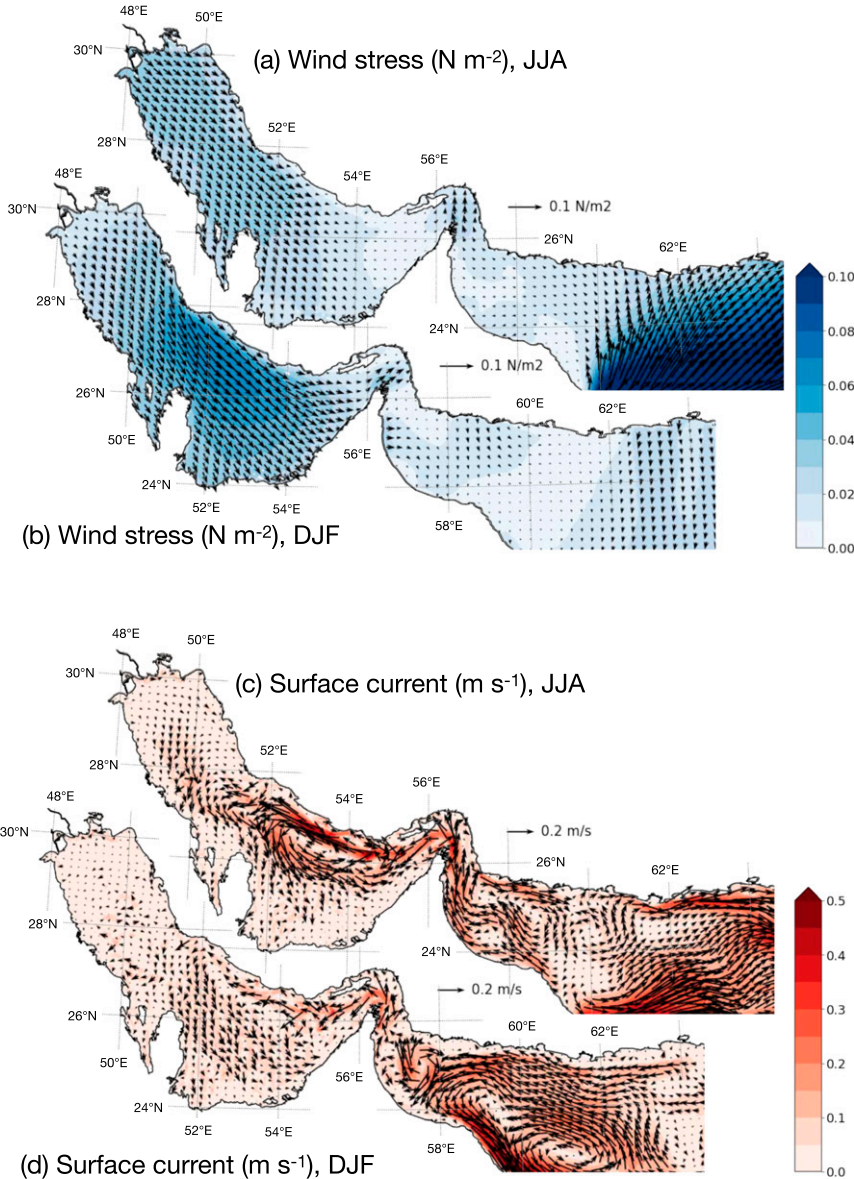
FIG. 4. (a),(b) Wind stress (N m^{-2}) and (c),(d) surface current (m s^{-1}) in summer [June–August (JJA)] in (a) and (c) and winter [December–February (DJF)] in (b) and (d). In all plots shading represents the magnitude of the vector field.

that on entry (Xue and Eltahir 2015). We now analyze this water-mass transformation process in the Gulf model following the framework set out in Walin (1982) and Marshall et al. (1999). This can be used to elegantly infer and quantify the processes sustaining the overturning circulation.

a. Theoretical framework

Following the line of reasoning in Marshall et al. (1999), let us consider the volume of fluid within a certain density class $\mathcal{R}_\sigma(\sigma, t)$ as sketched in Fig. 6 which shows potential density layers centered around σ outcropping at the surface within the Gulf and extending back out into the Sea of Oman. The volume

$\mathcal{R}_\sigma(\sigma, t)$ can be changed by a diapycnal volume flux $A(\sigma, t)$, normal to isopycnal surfaces defined in terms of the fluid velocity ($\mathbf{v}$) and the isopycnal velocity ($\mathbf{v}_\sigma$) normal to the σ surfaces:

$$A(\sigma, t) = \iint_{\mathcal{A}_\sigma(\sigma, t)} (\mathbf{v} - \mathbf{v}_\sigma) \cdot \hat{\mathbf{n}}_\sigma d\mathcal{A}, \qquad (1)$$

where $\mathcal{A}_\sigma(\sigma, t)$ is the area of isopycnal surface and $\hat{\mathbf{n}}_\sigma$ is a unit vector normal to the isopycnal surface directed from low to high values. A positive $\mathbf{v} \cdot \hat{\mathbf{n}}_\sigma$ and $\mathbf{v}_\sigma \cdot \hat{\mathbf{n}}_\sigma$ refer to the fluid and isopycnal velocity from lower- to higher-density classes, respectively. As defined in Eq. (1), $A(\sigma, t)$ is positive when there
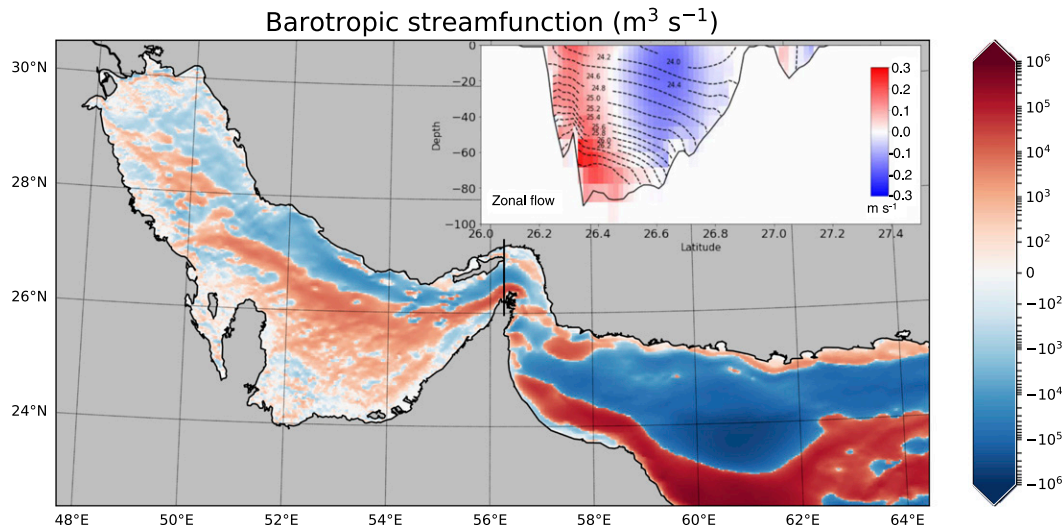
FIG. 5. Annually-averaged barotropic streamfunction ($m^3 s^{-1}$) plotted using a log scale (shading), with inset showing a vertical section of the annually-averaged zonal velocity across the Strait of Hormuz (south on the left). Positive streamfunction represents counterclockwise circulation. In the inset, positive zonal velocity is directed out of the Gulf. Also plotted in the inset are contours of isopycnals.

is a flux toward higher density since σ increases downward, as sketched in Fig. 6.

The evolution of σ itself is governed by the equation

$$\frac{\partial \sigma}{\partial t} = -\nabla \cdot (\mathbf{N}_\sigma + \sigma \mathbf{v}), \tag{2}$$

where $\mathbf{N}_\sigma$ is the nonadvective flux of σ, and $\sigma\mathbf{v}$ is the advective flux. As first shown by Walin (1982), $A(\sigma, t)$ can be precisely related to $B(\sigma, t)$, the nonadvective supply of buoyancy to the control volume $\mathcal{R}(\sigma, t)$, as follows (using the notation of Marshall et al. 1999)

$$A(\sigma, t) = \frac{\partial B(\sigma, t)}{\partial \sigma}, \tag{3}$$

where

$$B(\sigma, t) = -\iiint_{\mathcal{R}_\sigma(\sigma, t)} \nabla \cdot \mathbf{N}_\sigma dV \tag{4}$$

depends on $\mathbf{N}_\sigma$ acting on the boundaries of $\mathcal{R}_\sigma$.

Separating Eq. (3) into a part due to air–sea fluxes and a part due to diffusive, nonadvective fluxes acting in the interior ocean, it can be written

$$A = F - \frac{\partial D}{\partial \sigma}, \tag{5}$$

where

$$F = \frac{\partial B_s(\sigma, t)}{\partial \sigma} \tag{6}$$

depends only on surface fluxes and

$$D = \iint_{\mathcal{A}_\sigma} \mathbf{N}_\sigma \cdot \hat{\mathbf{n}}_\sigma d\mathcal{A} \tag{7}$$

depends on diffusive fluxes within the ocean.

The quantity F is called the "transformation rate." From Eq. (6), F can be written in a form convenient for computation, involving integration of air–sea fluxes over outcrops, thus,

$$B_s(\sigma, t) = -\frac{\rho_0}{g} \iint_{\mathcal{A}_s(\sigma, t)} \mathcal{B}_s d\mathcal{A}, \tag{8}$$

where $\mathcal{A}_s(\sigma, t)$ is the area of the sea surface with the density interval around σ at time t and
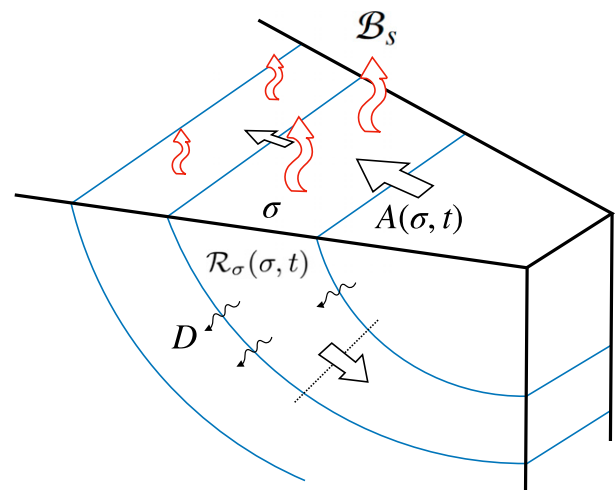

FIG. 6. Schematic showing potential density surfaces, σ, outcropping at the sea surface within the Gulf (for example) and extending back out into the Sea of Oman (σ increases with depth). The volume of fluid between adjacent σ surfaces $\mathcal{R}_\sigma(\sigma, t)$ can be changed by the divergence of a diapycnal volume flux $A(\sigma, t)$ normal to σ, which itself can be related to the air–sea buoyancy fluxes $\mathcal{B}_s$ and the diffusive buoyancy fluxes D acting on the σ surfaces that bound the volume, as expressed in Eqs. (5)–(9).

$$\mathcal{B}_s = \frac{g}{\rho_0}\left[\frac{\alpha}{c_w}(\mathcal{Q}_{SW} + \mathcal{Q}_{LW} + \mathcal{Q}_L + \mathcal{Q}_S) + \rho_0\beta S(E - P - R)\right] \quad (9)$$

is the air–sea buoyancy flux made up of its heat (first term in brackets on the right-hand side), and freshwater (second term in brackets on the right-hand side) contributions. Here, ρ_0 is the reference density; α is the thermal expansion coefficient for seawater; c_w is the heat capacity of water; $\mathcal{Q}_{SW}$, $\mathcal{Q}_{LW}$, $\mathcal{Q}_L$, and $\mathcal{Q}_S$ are the heat flux due to shortwave radiation, longwave radiation, latent heat and sensible heat, respectively; β is the haline contraction coefficient; S is the local surface salinity; and E, P, and R are evaporation, precipitation, and river runoff (m s^{-1}), respectively. Note that in the above formulas A and F have units of m^3s^{-1}, B_s has units of $(\text{kg m}^{-3}) \times (\text{m}^3\text{s}^{-1})$, and $\mathcal{B}_s$ has units of m^2s^{-3}.

At the surface of the ocean, if outcropping buoyancy surfaces lose increasingly more buoyancy at higher-density classes, then $\partial B_s(\sigma, t)/\partial\sigma > 0$, and a positive diapycnal volume flux is induced: in the absence of diffusive processes, fluid moves to heavier density classes. In this way, computing F for each density class at the surface enables us to probe the role of air–sea fluxes in sustaining the overturning circulation.

b. Diagnosis of water mass transformation in the model

We use MITgcm's capability to compute water-mass transformation rates as a function of density class. These diagnostics are obtained through use of the LAYERS package in which the theoretical framework described above is put into practice (see Abernathey et al. 2016). The analyzed density range is divided in layers from 22 to 42.1 kg m^{-3} with an interval of 0.15 kg m^{-3}. This encompasses most of the water mass in the domain, but occasionally density variations exceed this range, particularly in summer when evaporation increases density beyond 42.1 kg m^{-3}. When this occurs, water masses which lie outside the chosen range are merged to the closest density bin. LAYERS also computes the velocity within isopycnal layers allowing us to directly estimate the overturning circulation in the Gulf and Sea of Oman, as described in section 4c (see supporting information of Abernathey et al. 2016).

As shown in Fig. 7a, annually averaged water-mass transformation rates are positive in the Gulf, suggesting that the surface fluxes act to induce a flow toward higher-density classes. Since surface waters in the Gulf are generally denser than in the Sea of Oman (Fig. 7g) (Azhar et al. 2016), this implies water is being drawn into the Gulf by air–sea transformation within the Gulf. This is in contrast to the rather small transformation rates in the Sea of Oman. The central Gulf near the northern coast has the most active water-mass transformation, with values exceeding 125 m^3 s^{-1} (Fig. 7a). Here the contribution from the net heat flux dominates that from the freshwater flux (Figs. 7d,g). Heat loss increases the surface density resulting in a water-mass transformation rate which is positive over the interior of the Gulf. This should be contrasted with the transformation rate near the southern coast where evaporation E results in a net positive water-mass transformation (Figs. 7a,g), despite the warming effects of the net heat flux there (negative values in Fig. 7d). As a consequence, the net effect of air–sea fluxes over the Gulf is

to draw light water in through the Strait of Hormuz and make it denser.

The water-mass transformation rate exhibits opposite signs seasonally. In summer, the total surface flux creates a negative water-mass transformation rate that stems from the surface heat flux (Figs. 7b,e). Although the surface freshwater flux tends to increase the transformation rate, its contribution is considerably smaller than that from the surface heat flux (Figs. 7e,h). In winter, on the other hand, the water-mass transformation rate is positive at the surface to which both the surface heat and freshwater flux contribute (Figs. 7c,f,i). In particular, the contribution from the surface heat flux is the greatest and exceeds 400 m^3 s^{-1} in the central Gulf near the northern coast. The contribution from the freshwater flux is greater in winter than summer, suggesting more evaporation by the stronger surface wind (Fig. 4b).

According to Eq. (5), the water-mass transformation rate can be related to the diapycnal volume flux $A(\sigma, t)$ when the diffusive flux is ignored, and $A(\sigma, t)$ is determined by $\mathbf{v}$ and $\mathbf{v}_\sigma$. Since there is net inflow through the Strait of Hormuz near the surface (Figs. 4c,d), the $\mathbf{v} \cdot \hat{\mathbf{n}}_\sigma$ is positive (flowing toward higher-density class) in both summer and winter. The $\mathbf{v}_\sigma \cdot \hat{\mathbf{n}}_\sigma$, on the other hand, changes in sign over the season. As summer approaches, outcropping positions of isopycnals move into the Gulf (positive $\mathbf{v}_\sigma \cdot \hat{\mathbf{n}}_\sigma$) while the opposite occurs as winter approaches (negative $\mathbf{v}_\sigma \cdot \hat{\mathbf{n}}_\sigma$) (Figs. 7h,i). The positive $\mathbf{v} \cdot \hat{\mathbf{n}}_\sigma$ and negative $\mathbf{v}_\sigma \cdot \hat{\mathbf{n}}_\sigma$ in winter add up to make the positive water-mass transformation rate and volume flux. However in summer, the retreat speed of the outcropped isopycnal overwhelms the flow velocity. A rough estimate based on the position of the $\sigma = 26$ kg m^{-3} outcrop yields a $|\mathbf{v}_\sigma|$ of 0.04 m s^{-1}, which is roughly double the mean surface velocity near the Strait of Hormuz. As a result, the volume flux becomes negative even though the ocean current is directed toward higher-density classes in summer.

The water-mass transformation rate can be further visualized by dividing the Gulf on through the Strait of Hormuz into narrow bands that are ascribed numbers from 0 to 100 starting from the innermost region in the Gulf out through the Strait into the Sea of Oman (Fig. 7a). The transformation rate F is then averaged over these bands to yield Fig. 8 where the various contributions of the surface flux components presented in Eq. (9) are shown.

In summer, the contribution from the shortwave radiation dominates other surface forcing terms in the water-mass transformation rate (Fig. 8b). Upward longwave radiation and latent heat loss densify the surface ocean, but their combined contribution is still lower than that from the shortwave radiation. Although evaporation tends to increase the surface density, its contribution is considerably smaller than those from both longwave radiation and latent heat. The transformation rate by sensible heat flux is negative, indicating the air temperature is higher than SST in summer. Its size is comparable with that of evaporation near the northern end of the Gulf but approaches zero toward the Sea of Oman. The total water-mass transformation rate in the Gulf is negative, suggesting a diapycnal volume flux toward lower-density class. This negative volume flux does not necessarily mean the actual
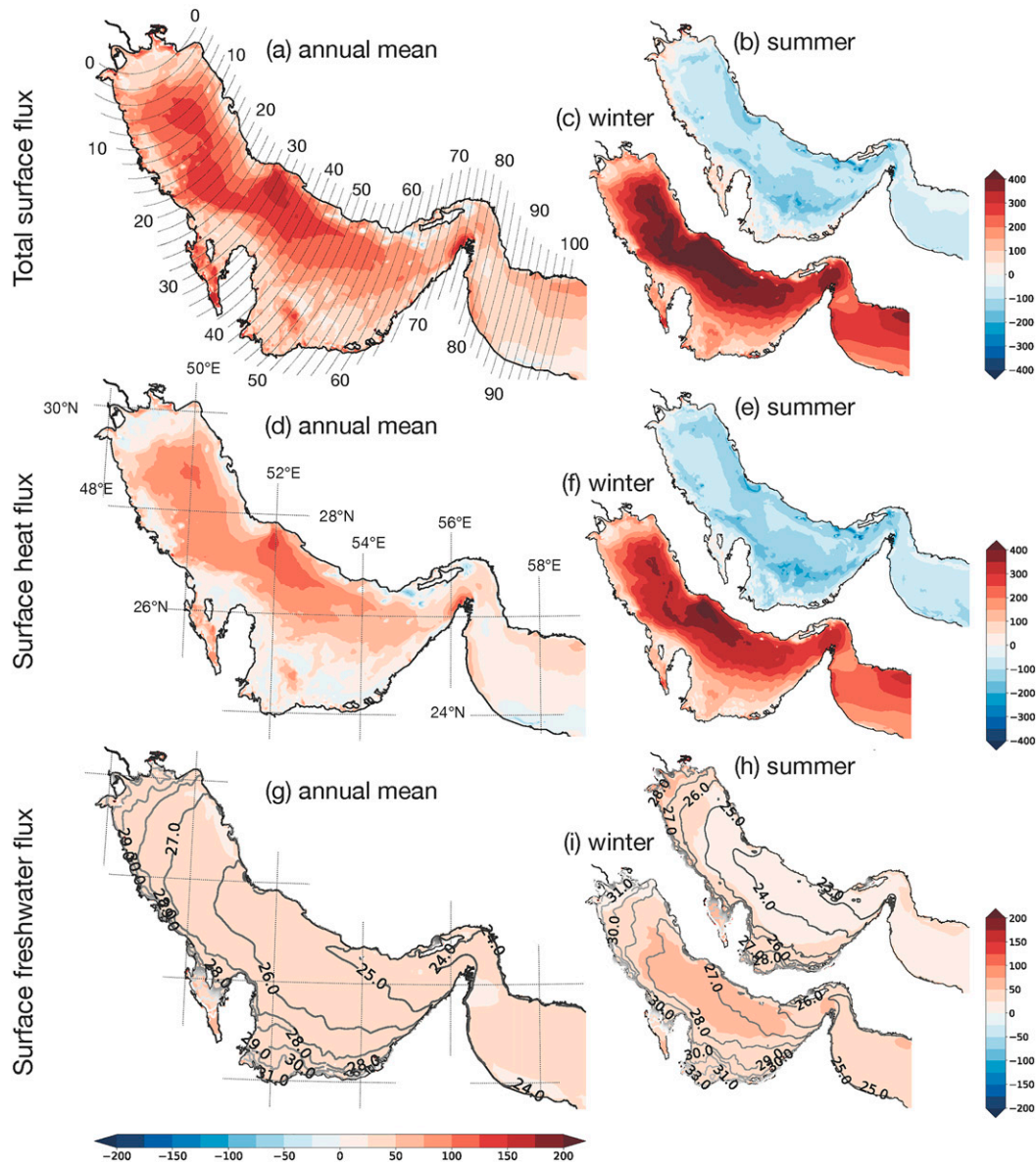
water-mass transformation rate (m³ s⁻¹)

FIG. 7. (a)–(c) Water-mass transformation rate, $F = \partial B_s(\sigma, t)/\partial\sigma$ (m³ s⁻¹), implied by air–sea buoyancy fluxes, together with separate contributions from (d)–(f) heat fluxes and (g)–(i) freshwater fluxes, as defined in (9). The annual mean transformation rates are shown in (a), (d), and (g) while those in summer and winter are in (b), (e), and (h) and (c), (f), and (i), respectively. The lines with numbers in (a) define the regions over which spatial averages are computed in the construction of Fig. 8. The contours in (g)–(h) represent isopycnals. Note that (a) = (d) + (g), (b) = (e) + (h), and (c) = (f) + (i). Also note that the color scale in (b), (c), (e), and (f) is different from others.

flow toward negative density class (out of the Gulf) because v_σ needs to be considered. As discussed above, the v and v_σ are both positive with v_σ being the larger, and Fig. 8b shows that the solar radiation is the main cause.

In winter, shortwave radiation tends to decrease surface density but its contribution is smaller than that in summer

(Fig. 8c). The contribution of upward longwave radiation also becomes smaller as SSTs cool down, but latent heat loss shows a greater positive contribution to the water-mass transformation rate compared to that in summer. In addition, sensible heat and evaporation both densify the surface instead of cancelling each other as in summer, contributing to the positive water-mass
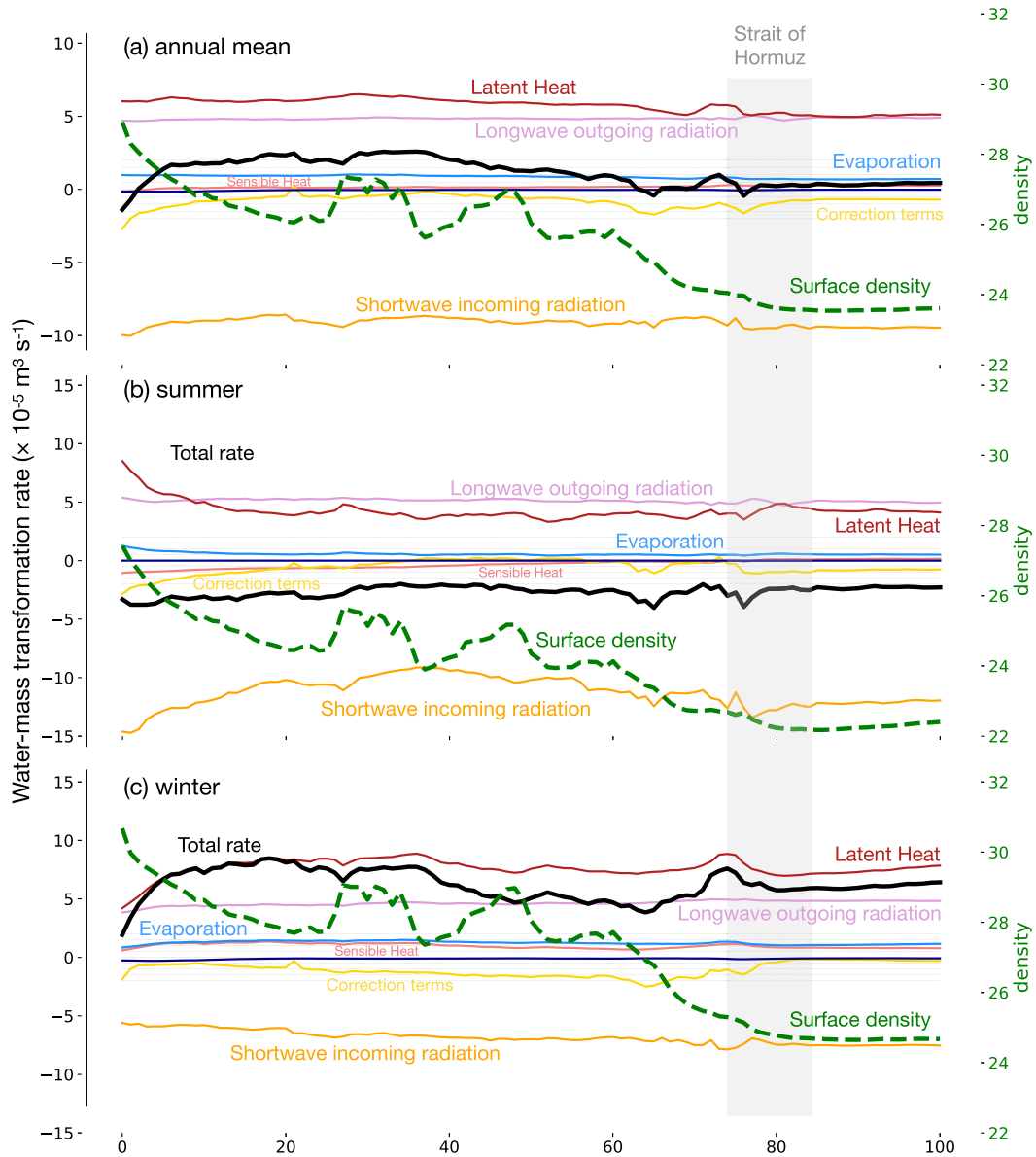
Partition of the water-mass transformation rate

FIG. 8. (a) Annual-mean, (b) summer-mean, and (c) winter-mean water-mass transformation rate (solid black lines) $F(\sigma)$ computed from Eq. (6) using (8) and (9). In each panel, the dashed line shows the surface density averaged in the sections numbered and shown in Fig. 7a. The number along the x axis indicates the location of the section along the Gulf increasing eastward. Positive values imply a tendency to induce a diapycnal volume transport directed toward higher densities. Points shallower than 20 m are excluded in the average. The contributions from precipitation and river runoff are close to zero and hence not shown.

transformation rate. As a result, the total rate is positive in the Gulf and Sea of Oman, indicating a volume flux into the Gulf. In this season, positive v and negative v_σ make the volume flux positive and greater in size, and the latent heat loss makes the greatest contribution.

In the annual average, the Gulf has a positive water-mass transformation rate (Fig. 8a). The heat gain from shortwave radiation is the largest contributor to the water-mass

transformation, but combined contribution from outgoing longwave radiation and the latent heat loss exceeds it (Fig. 8a). Evaporation exceeds precipitation (not shown as it is close to zero) thus increasing the density of surface waters in the Gulf (Swift and Bower 2003; Kämpf and Sadrinasab 2006). However, its impact is approximately 5 times smaller than that of latent heat loss, the single largest contributor to a positive water-mass transformation. The annual mean of sensible heat
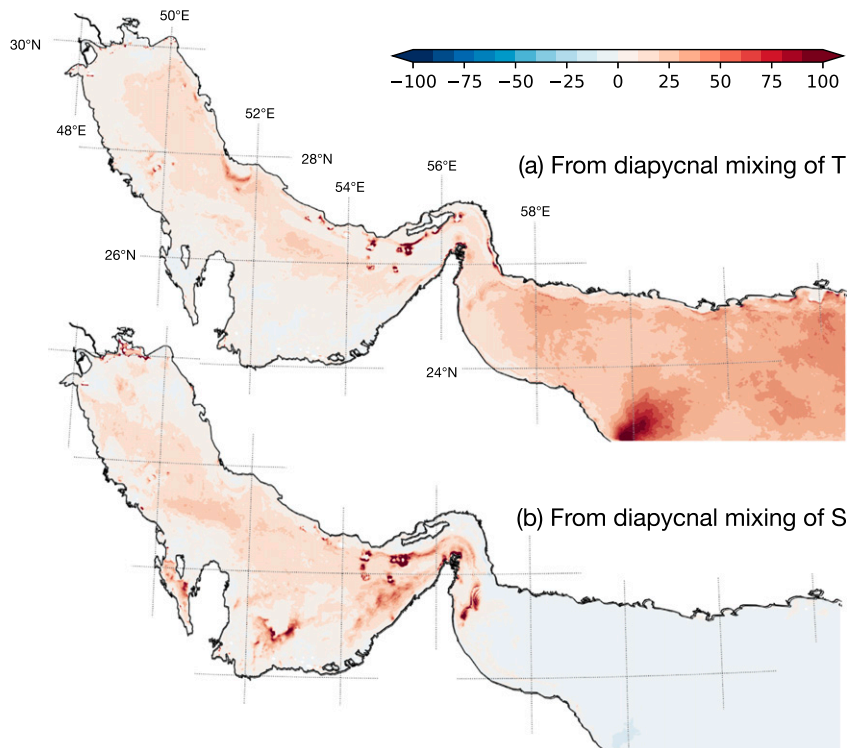
Annually averaged water-mass transformation rate (m³ s⁻¹)

FIG. 9. Annual mean volume flux contributed by diapycnal mixing of (a) temperature and (b) salinity integrated over the depth of the water column. The rate is weighted by the grid area. Note that the color scale is slightly different from Fig. 7, to enable details to be seen in the Gulf, although generally they are very much smaller than that due to air–sea interaction.

flux is close to zero, and its contribution to the density increase is the smallest. A linear free surface formulation introduces a surface correction term for the local conservation of tracers (Campin et al. 2004) and has a net negative effect on transformation rate (Fig. 8). Although these correction terms are not small enough to be neglected, we will not discuss them further since they are not directly related to surface fluxes.

The volume flux across isopycnals may converge or diverge fluid into a certain density class, leading to inflation or deflation of the volume of fluid within the layer. The formation rate—the volume squeezed into a layer—can be computed as $\partial A/\partial \sigma$ (Marshall et al. 1999). In Fig. 8a the water-mass transformation rate F is plotted against distance rather than density because, although there is a generally monotonic relationship between surface density and distance into the Gulf, the same density can be found in multiple places. Although, for this reason, the formation rate cannot be obtained quantitatively from Fig. 8a, we can still qualitatively describe it by inspecting the transformation rate and surface density together.

The surface density tends to increase toward the lower bin number (see the green dashed line in Fig. 8 and surface density plotted in Figs. 7g–i), indicating a volume flux toward the northwest. The annual mean transformation rate is positive in the interior and rapidly decreases near the innermost part of the Gulf. There is thus a convergence of F toward the end of the

Gulf which results in a creation of the most dense water mass there. The rapid decrease in the transformation rate is clearer in winter (Fig. 8c). It is related to the reduced contribution from latent heat loss near the innermost part of the Gulf in winter, which can be explained by reduced of wind stress (Fig. 4b). In summer, the water-mass transformation rate is rather constant although there is a slight decrease near the end of the Gulf. The convergence of F near the innermost part of the Gulf in both seasons is broadly consistent with the vertical sections of density; the isopycnals are rather vertical as the result of water formation due to the convergence of surface water mass (Figs. 3f and 2f).

The density at the surface can also be changed by diapycnal diffusive flux occurring within the ocean (Marshall et al. 1999). The diapycnal diffusive flux can also be partitioned into heat and salt diffusion, and both make a positive contribution to the transformation in the Gulf (Fig. 9). It indicates that the vertical mixing provides cold and salty subsurface water to the surface layer and increases the density. However, the transformation rates due to these diffusive fluxes make a generally smaller contribution than surface fluxes. They are generally lower than $20\,\mathrm{m^3\,s^{-1}}$ in the Gulf except in the limited local regions where the diapycnal diffusive salinity flux approaches $100\,\mathrm{m^3\,s^{-1}}$. In other words, Fig. 9 suggests that water mass transformation by the parameterized
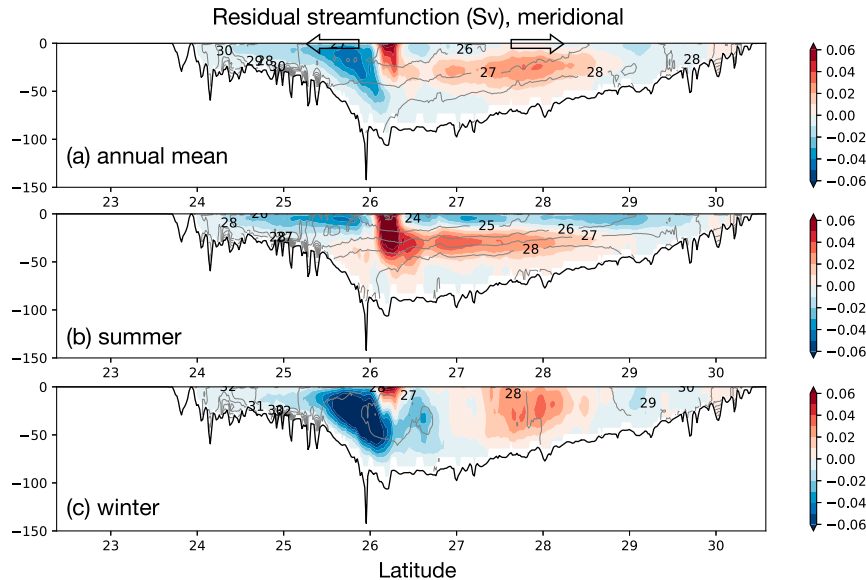
FIG. 10. The residual overturning streamfunction (Sv; shading) in the (a) annual mean, (b) summer, and (c) winter. The Gulf and Sea of Oman are shown separately at the left- and right-hand side, respectively. Arrows in (a) represent the direction of the overturning circulation. Isopycnals are also plotted in gray with an interval of 1 kg m^{-3}. Negative streamfunction values represent anticlockwise circulation, while positive values induce clockwise circulation. It should be noted that two different color scales (Sv) are used inside and outside of the Gulf in (a). The bathymetry shows the deepest depth along latitude.

background diapycnal diffusivity is small, yet larger, localized transformation can occur where the KPP boundary layer scheme can generate significantly enhanced localized diffusivities.

c. Overturning circulation in the Gulf

The overturning circulation can be quantified using the velocity in the layer defined by isopycnals. If the thickness of a certain layer is h, and the zonal velocity in that layer is u, the residual-mean zonal velocity in that layer can be calculated thus (see, e.g., Pinardi et al. 2019):

$$\frac{\overline{uh}}{\overline{h}} = \overline{u} + \frac{\overline{u'h'}}{\overline{h}}, \tag{10}$$

where the overbar refers to a time and meridional average while the prime is the deviation from that average. We analyze the annually averaged residual overturning circulation, associated with the left-hand-side term in Eq. (10), in the Gulf and the Sea of Oman by making use of the currents projected along isopycnals, provided by the LAYERS diagnostic package of MITgcm. The result is remapped into z space for viewing by finding the depth for each density class at a given grid. Note that the diagnostics are computed online and thus includes transports of all resolved scales (including tides and eddies). In particular, it should be noted that the residual circulation is not the Eulerian-mean overturning circulation associated with the first term in the right-hand side of Eq. (10), as discussed in the context of the Antarctic Circumpolar Current in, for example, Marshall and Radko

(2003). We explore both zonal and meridional overturning cells in the annual mean, and in the winter and summer. The streamfunction is defined such that there is counterclockwise circulation around negative values.

The overturning circulation in the zonal direction highlights the flow through the Strait of Hormuz where the core of the inflow and outflow is found at the surface and near the bottom, respectively (Fig. 10). The direction of the zonal overturning circulation confirms inflow of relatively freshwater from the Sea of Oman into the Gulf. The overturning circulation in the Sea of Oman has clear seasonality; Fig. 10b shows the upwelling due to the southwesterly wind in summer (Fig. 4a) that is not apparent in winter (Beal et al. 2013) (Fig. 10c). The overturning circulation is generally weaker within the Gulf than outside it—note the different scales inside and outside. The zonal residual streamfunction indicates that the surface inflow weakens and subducts at approximately east of 50°E in the annual mean. This characteristic of the surface current is also consistent with a convergence of the water-mass transformation rate (Fig. 8) seen near bin number 10 corresponding to roughly 50°E. The penetration is weaker in winter, which is consistent with the wind stress pattern in the Gulf (Figs. 4a,b). The overturning circulation in the Gulf is more clearly defined in summer when the water is stratified (Fig. 10b). In contrast, the wintertime convection in the Gulf tends to homogenize the water mass, resulting in a somewhat more patchy overturning circulation. Nevertheless, the water mass formation near the innermost part of the Gulf is present in the wintertime zonal overturning circulation (Fig. 10c). The outflow at depth enters the Sea of Oman and finds its neutral
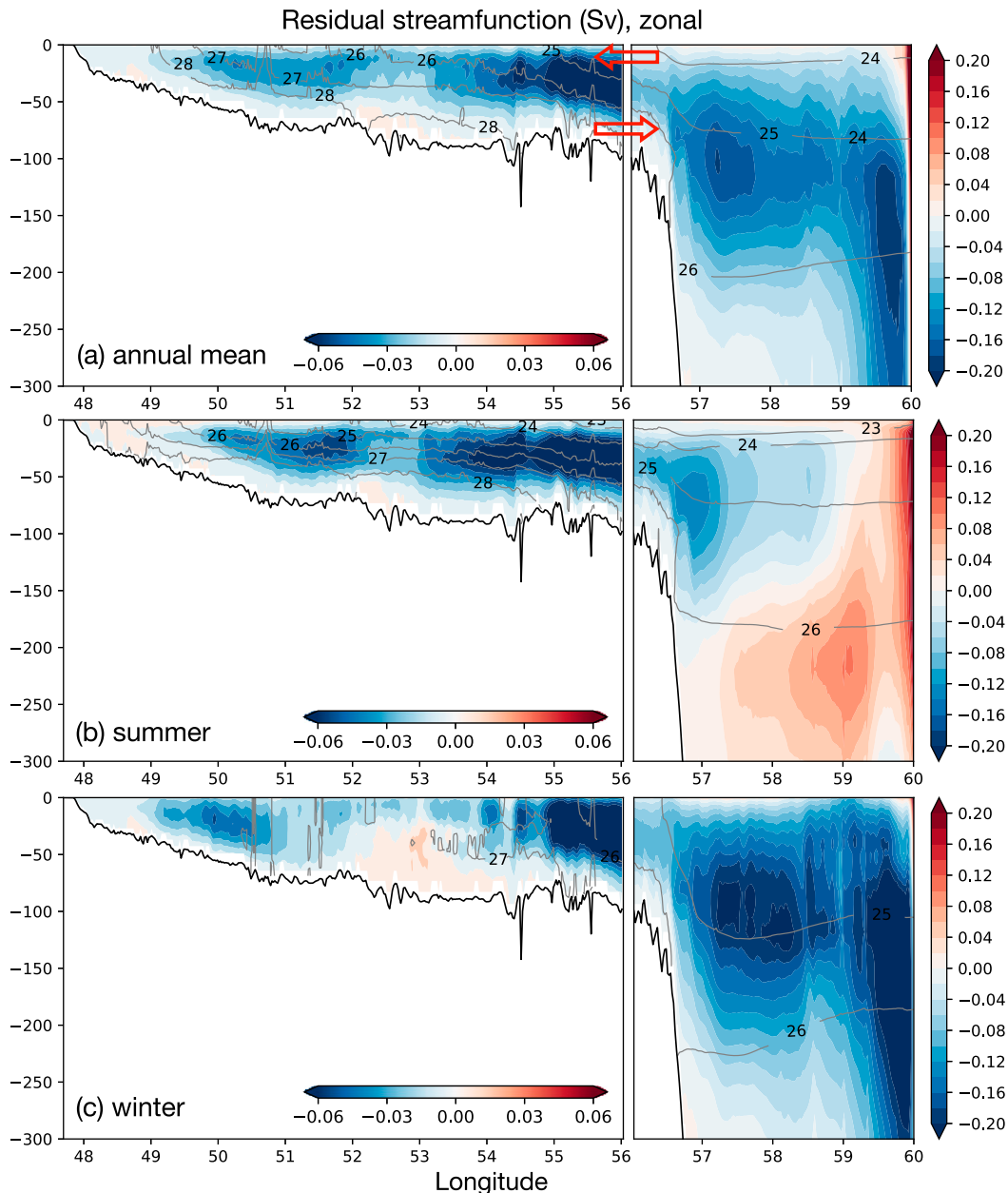
FIG. 11. The meridional residual overturning streamfunction (Sv; shading) in the (a) annual mean, (b) summer, and (c) winter. Only the Gulf (west of 56°) is considered. Arrows in (c) represent the direction of the overturning circulation. Isopycnals are also plotted in gray with an interval of 1 kg m^{-3}. Please refer to Fig. 10 for more detailed explanations.

level near 200 m or so and spreads eastward, although it is sensitive to the season.

The meridional residual streamfunction further inside the Gulf exhibits considerable seasonality (Fig. 11). In the annually averaged streamfunction shown in Fig. 11a, positive values north of 27°N (<0.04 Sv) suggests that the surface current is directed toward the northern part of the Gulf while negative values to the south of 26°N (>−0.05 Sv) indicates surface southward flow. The overturning cell in summer shows a two-cell structure north of 26.5°N; a relatively thin negative (counterclockwise) streamfunction near the surface that lies above a positive streamfunction (Fig. 11b). The counterclockwise circulation comprises surface flow toward the center and subsurface flow toward the north end of the Gulf. In winter, the near-surface negative streamfunction disappears as the lower cell extends up to the surface (Fig. 11c). Convection in the northern part of the Gulf provides water with density greater than 28 kg m^{-3} that can be seen near the bottom in summer. The circulation pattern in the southern part of the Gulf agrees with both the direction of the seasonal surface current and the barotropic streamfunction, with southeastward surface flow (Figs. 4 and 5). The positive streamfunction near

26.2°N has its maximum at the surface, suggesting southward flow. Both the southwestward inflow through the Strait of Hormuz and the counterclockwise circulation at the central Gulf contribute to this positive streamfunction. Indeed, the positive streamfunction is apparent more in summer (Fig. 11b) when the counterclockwise circulation is better developed at the central Gulf (Figs. 4c,d). In summary, broad consistency between the overturning circulation and water-mass transformation rate demonstrates a satisfying connection between air–sea buoyancy fluxes and the general circulation in the Gulf.

5. Discussion and conclusions

The Arabian Gulf is a semiclosed evaporative basin in which relatively fresh water is supplied near the surface through the Strait of Hormuz while salty water exits the Gulf at depth. The differing salinities between the inflow and outflow at the Strait suggests that water-mass transformation rate must be positive within the Gulf with the density of the water being increased. Surface fluxes are responsible for this densification, but the detailed processes of water-mass transformation and resulting overturning circulation are complex and not fully documented or understood (Yao 2008). We have made use of the MITgcm and its diagnostic capabilities (Abernathey et al. 2016; Doddridge et al. 2019) to explore these processes in a novel and hopefully illuminating way.

The circulation derived from our 1/48° resolution model is depicted as follows. The surface flow is characterized by inflow through the Strait of Hormuz and cyclonic circulation on the eastern margin of the Gulf feeding outflow toward the Sea of Oman. The northwest region of the Gulf comprises a current flowing toward the center of the Gulf, particularly in summer. In the central Gulf, air–sea heat flux is the main cause of densification. Surface density decrease due to solar heating is counterbalanced by both upward longwave radiation and latent heat loss in the annual mean. In particular, latent heat loss is the largest contributor to density increase and this contribution is 5 times larger than evaporation to water-mass transformation (Fig. 8). Densification of surface waters close to the southern coast, instead, is mainly driven by evaporation (Fig. 7) and sinks to depth. It then exits the Gulf through the southern portion of the Strait of Hormuz, finding its level at 200 m or so in the Sea of Oman.

The water-mass transformation rate exhibits clear seasonality with changes in v_σ, induced by the cycle of warming and cooling, playing an important role. However, although v_σ has a significant impact on the seasonal diapycnal volume flux, it does not contribute to the annually averaged volume flux since the annual mean of v_σ is close to zero.

The circulation within the Gulf is in accord with expectations based on water-mass transformation theory (Walin 1982; Marshall et al. 1999). Positive annually averaged water-mass transformation rates due to surface fluxes (Figs. 7a,d,g) imply a diapycnal volume flux toward higher densities at the inner Gulf. There exists the convergence of water-mass transformation rates near the innermost part of the Gulf. This implies the water-mass formation and subsequent downwelling. The

zonal and meridional overturning circulation support the circulation patterns anticipated by the water-mass transformation rate theory. The annually averaged volume flux through the Strait of Hormuz in our calculations is somewhat larger than 0.14 Sv, similar to the previously reported values (Johns et al. 2003; Vasou et al. 2020).

Our study suggests that, because the contribution to the transformation rate by interior diffusive fluxes is so much smaller than that due to air–sea fluxes, the transformation can be inferred to a good approximation directly from air–sea fluxes. This implies that any changes in air–sea fluxes will modify the overturning circulation. The 2-m temperature over the Gulf shows a positive trend ($\approx$0.3°C decade^{-1}), (Patlakas et al. 2019), and sea surface temperatures are also warming (Shirvani et al. 2015; Noori et al. 2019). Along with this warming trend, the freshwater flux also varies in time (Campos et al. 2020). The warming trend, coupled with a net negative freshwater flux ($E - P$) over the Gulf, will likely continue into the future (Kirtman et al. 2013). Wind changes may also be important since they are intimately involved in setting patterns and magnitudes of surface fluxes. Our study therefore sets out a clear analysis method for understanding and perhaps predicting such changes. This will be the topic of future research.

Finally, our experiment design also provides a comprehensive framework from which to compute the impact of desalination plants on oceanic circulation in the Gulf. The lives of people living around the Gulf depend on a supply of freshwater provided by desalination facilities. During the desalination process, freshwater is removed from seawater and brine is discharged back to the Gulf. This can result in an increase in salinity which is twice as high as the water drawn into the facilities (Bashitialshaaer et al. 2011). The discharge typically occurs near the surface and acts as a negative freshwater flux (Ibrahim and Eltahir 2019). According to the water-mass transformation framework employed here, desalination plants will contribute to an enhancement of water-mass formation near the coastal region, inducing stronger sinking. This will likely strengthen the overturning circulation and enhance the inflow through the Strait of Hormuz. As more desalination facilities are anticipated in the future, likely changes in overturning circulation could be estimated using the approach outlined here.

Data availability statement. The full LLC4320 model setup with compile-time and run-time parameters can be found at http://wwwcvs.mitgcm.org/viewvc/MITgcm/MITgcm_contrib/llc_hires/llc_4320/.

REFERENCES

Abernathey, R. P., I. Cerovecki, P. R. Holland, E. Newsom, M. Mazloff, and L. D. Talley, 2016: Water-mass transformation

by sea ice in the upper branch of the Southern Ocean overturning. *Nat. Geosci.*, **9**, 596–601, https://doi.org/10.1038/ngeo2749.

Alessi, C. A., H. D. Hunt, and A. S. Bower, 1999: Hydrographic data from the US naval oceanographic office: Persian Gulf, Southern Red Sea, and Arabian Sea 1923-1996. Woods Hole Oceanographic Institution Tech. Rep. WHOI-99-02, 70 pp., https://www2.whoi.edu/site/bower-lab/wp-content/uploads/sites/12/2018/03/TechRpt_HydrographicDAta.pdf.

Alosairi, Y., and T. Pokavanich, 2017: Residence and transport time scales associated with Shatt Al-Arab discharges under various hydrological conditions estimated using a numerical model. *Mar. Pollut. Bull.*, **118**, 85–92, https://doi.org/10.1016/j.marpolbul.2017.02.039.

——, J. Imberger, and R. A. Falconer, 2011: Mixing and flushing in the Persian Gulf (Arabian Gulf). *J. Geophys. Res.*, **116**, C03029, https://doi.org/10.1029/2010JC006769.

Azam, M. H., W. Elshorbagy, T. Ichikawa, T. Terasawa, and K. Taguchi, 2006: 3D model application to study residual flow in the Arabian Gulf. *J. Waterw. Port. Coast. Ocean Eng.*, **132**, 388–400, https://doi.org/10.1061/(ASCE)0733-950X(2006)132:5(388).

Azhar, M. A., M. Temimi, J. Zhao, and H. Ghedira, 2016: Modeling of circulation in the Arabian Gulf and the Sea of Oman: Skill assessment and seasonal thermohaline structure. *J. Geophys. Res. Oceans*, **121**, 1700–1720, https://doi.org/10.1002/2015JC011038.

Badin, G., R. G. Williams, Z. Jing, and L. Wu, 2013: Water mass transformations in the southern ocean diagnosed from observations: Contrasting effects of air–sea fluxes and diapycnal mixing. *J. Phys. Oceanogr.*, **43**, 1472–1484, https://doi.org/10.1175/JPO-D-12-0216.1.

Bashitialshaaer, R., K. M. Persson, and M. Aljaradin, 2011: Estimated future salinity in the Arabian Gulf, the Mediterranean Sea and the Red Sea consequences of brine discharge from desalination. *Int. J. Acad. Res.*, **3**, 133–140.

Beal, L. M., V. Hormann, R. Lumpkin, and G. R. Foltz, 2013: The response of the surface circulation of the Arabian Sea to monsoonal forcing. *J. Phys. Oceanogr.*, **43**, 2008–2022, https://doi.org/10.1175/JPO-D-13-033.1.

Campin, J.-M., A. Adcroft, C. Hill, and J. Marshall, 2004: Conservation of properties in a free-surface model. *Ocean Modell.*, **6**, 221–244, https://doi.org/10.1016/S1463-5003(03)00009-X.

Campos, E. J. D., A. L. Gordon, B. Kjerfve, F. Vieira, and G. Cavalcante, 2020: Freshwater budget in the Persian (Arabian) Gulf and exchanges at the Strait of Hormuz. *PLOS ONE*, **15**, e0233090, https://doi.org/10.1371/journal.pone.0233090.

Cerovečki, I., and M. R. Mazloff, 2016: The spatiotemporal structure of diabatic processes governing the evolution of subantarctic mode water in the Southern Ocean. *J. Phys. Oceanogr.*, **46**, 683–710, https://doi.org/10.1175/JPO-D-14-0243.1.

Chao, S.-Y., T. W. Kao, and K. R. Al-Hajri, 1992: A numerical investigation of circulation in the Arabian Gulf. *J. Geophys. Res.*, **97**, 11 219–11 236, https://doi.org/10.1029/92JC00841.

Daru, V., and C. Tenaud, 2004: High order one-step monotonicity-preserving schemes for unsteady compressible flow calculations. *J. Comput. Phys.*, **193**, 563–594, https://doi.org/10.1016/j.jcp.2003.08.023.

Doddridge, E. W., J. Marshall, H. Song, J.-M. Campin, M. Kelley, and L. Nazarenko, 2019: Eddy compensation dampens Southern Ocean sea surface temperature response to westerly wind trends. *Geophys. Res. Lett.*, **46**, 4365–4377, https://doi.org/10.1029/2019GL082758.

Egbert, G., and S. Erofeeva, 2002: Efficient inverse modeling of barotropic ocean tides. *J. Atmos. Oceanic Technol.*, **19**, 183–204, https://doi.org/10.1175/1520-0426(2002)019<0183:EIMOBO>2.0.CO;2.

Garrett, C., K. Speer, and E. Tragou, 1995: The relationship between water mass formation and the surface buoyancy flux, with application to Phillips' Red Sea model. *J. Phys. Oceanogr.*, **25**, 1696–1705, https://doi.org/10.1175/1520-0485(1995)025<1696:TRBWMF>2.0.CO;2.

Hosseinibalam, F., S. Hassanzadeh, and A. Rezaei-Latifi, 2011: Three-dimensional numerical modeling of thermohaline and wind-driven circulations in the Persian Gulf. *Appl. Math. Model.*, **35**, 5884–5902, https://doi.org/10.1016/j.apm.2011.05.040.

Ibrahim, H. D., and E. A. B. Eltahir, 2019: Impact of brine discharge from seawater desalination plants on Persian/Arabian Gulf salinity. *J. Environ. Eng.*, **145**, 04019084, https://doi.org/10.1061/(ASCE)EE.1943-7870.0001604.

Johns, W. E., F. Yao, D. B. Olson, S. A. Josey, J. P. Grist, and D. A. Smeed, 2003: Observations of seasonal exchange through the Straits of Hormuz and the inferred heat and freshwater budgets of the Persian Gulf. *J. Geophys. Res.*, **108**, 3391, https://doi.org/10.1029/2003JC001881.

Kämpf, J., and M. Sadrinasab, 2006: The circulation of the Persian Gulf: A numerical study. *Ocean Sci.*, **2**, 27–41, https://doi.org/10.5194/os-2-27-2006.

Kirtman, B., and Coauthors, 2013: Near-term climate change: Projections and predictability. *Climate Change 2013: The Physical Science Basis*, T. F. Stocker et al., Eds., Cambridge University Press, 953–1028.

Large, W. G., and S. Pond, 1981: Open ocean momentum flux measurements in moderate to strong winds. *J. Phys. Oceanogr.*, **11**, 324–336, https://doi.org/10.1175/1520-0485(1981)011<0324:OOMFMI>2.0.CO;2.

——, and A. G. Nurser, 2001: Ocean surface water mass transformation. *Ocean Circulation and Climate*, G. Siedler, J. Church, and J. Gould, Eds., International Geophysics Series, Vol. 77, Academic Press, 317–336, https://doi.org/10.1016/S0074-6142(01)80126-1.

——, J. McWilliams, and S. Doney, 1994: Oceanic vertical mixing: A review and a model with nonlocal boundary layer parameterization. *Rev. Geophys.*, **32**, 363–403, https://doi.org/10.1029/94RG01872.

Madani, L., A. Bidokhti, and M. Ezam, 2012: Estimation of salinity, heat and buoyancy budgets of the inflow coastal current into the Persian Gulf from the Strait of Hormuz. *Int. J. Mar. Sci. Eng.*, **2**, 107–114.

Marshall, J., and T. Radko, 2003: Residual-mean solutions for the Antarctic circumpolar current and its associated overturning circulation. *J. Phys. Oceanogr.*, **33**, 2341–2354, https://doi.org/10.1175/1520-0485(2003)033<2341:RSFTAC>2.0.CO;2.

——, A. Adcroft, C. Hill, L. Perelman, and C. Heisey, 1997a: A finite-volume, incompressible Navier Stokes model for studies of the ocean on parallel computers. *J. Geophys. Res.*, **102**, 5753–5766, https://doi.org/10.1029/96JC02775.

——, C. Hill, L. Perelman, and A. Adcroft, 1997b: Hydrostatic, quasi-hydrostatic, and nonhydrostatic ocean modeling. *J. Geophys. Res.*, **102**, 5733–5752, https://doi.org/10.1029/96JC02776.

——, D. Jamous, and J. Nilsson, 1999: Reconciling thermodynamic and dynamic methods of computation of water-mass transformation rates. *Deep-Sea Res. I*, **46**, 545–572, https://doi.org/10.1016/S0967-0637(98)00082-X.

Menemenlis, D., J. Campin, P. Heimbach, C. Hill, T. Lee, A. Nguyen, M. Schodlok, and H. Zhang, 2008: ECCO2: High resolution global ocean and sea ice data synthesis. *Mercator Ocean Quarterly Newsletter*, No. 31, Mercator Ocean, Toulouse,

France, 13–21, https://www.mercator-ocean.fr/wp-content/uploads/2015/06/lettre_31_en.pdf.

Nishikawa, S., H. Tsujino, K. Sakamoto, and H. Nakano, 2013: Diagnosis of water mass transformation and formation rates in a high-resolution GCM of the North Pacific. *J. Geophys. Res. Oceans*, **118**, 1051–1069, https://doi.org/10.1029/2012JC008116.

Noori, R., F. Tian, R. Berndtsson, M. R. Abbasi, M. V. Naseh, A. Modabberi, A. Soltani, and B. Kløve, 2019: Recent and future trends in sea surface temperature across the Persian Gulf and Gulf of Oman. *PLOS ONE*, **14**, e0212790, https://doi.org/10.1371/journal.pone.0212790.

Patlakas, P., C. Stathopoulos, H. Flocas, C. Kalogeri, and G. Kallos, 2019: Regional climatic features of the Arabian Peninsula. *Atmosphere*, **10**, 220, https://doi.org/10.3390/atmos10040220.

Pinardi, N., P. Cessi, F. Borile, and C. L. P. Wolfe, 2019: The Mediterranean Sea overturning circulation. *J. Phys. Oceanogr.*, **49**, 1699–1721, https://doi.org/10.1175/JPO-D-18-0254.1.

Pous, S., X. J. Carton, and P. Lazure, 2013: A process study of the wind-induced circulation in the Persian Gulf. *Open J. Mar. Sci.*, **3**, 27160, https://doi.org/10.4236/ojms.2013.31001.

——, P. Lazure, and X. Carton, 2015: A model of the general circulation in the Persian Gulf and in the Strait of Hormuz: Intraseasonal to interannual variability. *Cont. Shelf Res.*, **94**, 55–70, https://doi.org/10.1016/j.csr.2014.12.008.

Reynolds, M. R., 1993: Physical oceanography of the Gulf, Strait of Hormuz, and the Gulf of Oman—Results from the Mt Mitchell expedition. *Mar. Pollut. Bull.*, **27**, 35–59, https://doi.org/10.1016/0025-326X(93)90007-7.

Rocha, C. B., T. K. Chereskin, S. T. Gille, and D. Menemenlis, 2016: Mesoscale to submesoscale wavenumber spectra in drake passage. *J. Phys. Oceanogr.*, **46**, 601–620, https://doi.org/10.1175/JPO-D-15-0087.1.

Sadrinasab, M., and J. Kämpf, 2004: Three-dimensional flushing times of the Persian Gulf. *Geophys. Res. Lett.*, **31**, L24301, https://doi.org/10.1029/2004GL020425.

Schott, F. A., and J. P. McCreary, 2001: The monsoon circulation of the Indian Ocean. *Prog. Oceanogr.*, **51**, 1–123, https://doi.org/10.1016/S0079-6611(01)00083-0.

Shirvani, A., M. J. Nazemosadat, and E. Kahya, 2015: Analyses of the Persian Gulf sea surface temperature: Prediction and detection of climate change signals. *Arab. J. Geosci.*, **8**, 2121–2130, https://doi.org/10.1007/s12517-014-1278-1.

Smith, W. H. F., and D. T. Sandwell, 1997: Global seafloor topography from satellite altimetry and ship depth soundings. *Science*, **277**, 1956–1962, https://doi.org/10.1126/science.277.5334.1956.

Speer, K., and E. Tziperman, 1992: Rates of water mass formation in the North Atlantic Ocean. *J. Phys. Oceanogr.*, **22**, 93–104, https://doi.org/10.1175/1520-0485(1992)022<0093:ROWMFI>2.0.CO;2.

Stammer, D., K. Ueyoshi, A. Köhl, W. G. Large, S. A. Josey, and C. Wunsch, 2004: Estimating air–sea fluxes of heat, freshwater, and momentum through global ocean data assimilation. *J. Geophys. Res.*, **109**, C05023, https://doi.org/10.1029/2003JC002082.

Swift, S. A., and A. S. Bower, 2003: Formation and circulation of dense water in the Persian/Arabian Gulf. *J. Geophys. Res.*, **108**, 3004, https://doi.org/10.1029/2002JC001360.

Thoppil, P. G., and P. J. Hogan, 2010a: A modeling study of circulation and eddies in the Persian Gulf. *J. Phys. Oceanogr.*, **40**, 2122–2134, https://doi.org/10.1175/2010JPO4227.1.

——, and ——, 2010b: Persian Gulf response to a wintertime shamal wind event. *Deep-Sea Res. I*, **57**, 946–955, https://doi.org/10.1016/j.dsr.2010.03.002.

Torres, H. S., P. Klein, D. Menemenlis, B. Qiu, Z. Su, J. Wang, S. Chen, and L.-L. Fu, 2018: Partitioning ocean motions into balanced motions and internal gravity waves: A Modeling study in anticipation of future space missions. *J. Geophys. Res. Oceans*, **123**, 8084–8105, https://doi.org/10.1029/2018JC014438.

Tziperman, E., 1986: On the role of interior mixing and air–sea fluxes in determining the stratification and circulation of the oceans. *J. Phys. Oceanogr.*, **16**, 680–693, https://doi.org/10.1175/1520-0485(1986)016<0680:OTROIM>2.0.CO;2.

Vasou, P., V. Vervatis, G. Krokos, I. Hoteit, and S. Sofianos, 2020: Variability of water exchanges through the Strait of Hormuz. *Ocean Dyn.*, **70**, 1053–1065, https://doi.org/10.1007/s10236-020-01384-2.

Walin, G., 1982: On the relation between sea-surface heat flow and thermal circulation in the ocean. *Tellus*, **34**, 187–195, https://doi.org/10.3402/tellusa.v34i2.10801.

Wang, J., L. Fu, B. Qiu, D. Menemenlis, J. Farrar, Y. Chao, A. Thompson, and M. Flexas, 2018: An observing system simulation experiment for the calibration and validation of the surface water ocean topography sea surface height measurement using in situ platforms. *J. Atmos. Oceanic Technol.*, **35**, 281–297, https://doi.org/10.1175/JTECH-D-17-0076.1.

Xue, P., and E. A. B. Eltahir, 2015: Estimation of the heat and water budgets of the Persian (Arabian) Gulf using a regional climate model. *J. Climate*, **28**, 5041–5062, https://doi.org/10.1175/JCLI-D-14-00189.1.

Yao, F., 2008: Water mass formation and circulation in the Persian Gulf and water exchange with the Indian Ocean. Ph.D. thesis, University of Miami, 144 pp., https://scholarship.miami.edu/esploro/outputs/doctoral/Water-Mass-Formation-and-Circulation-in-the-Persian-Gulf-and-Water-Exchange-with-the-Indian-Ocean/991031447174202976.

——, and W. E. Johns, 2010: A HYCOM modeling study of the Persian Gulf: 2. Formation and export of Persian Gulf Water. *J. Geophys. Res.*, **115**, C11018, https://doi.org/10.1029/2009JC005788.